

UC Berkeley

UC Berkeley Previously Published Works

Title

Atmospheric teleconnection mechanisms of extratropical North Atlantic SST influence on Sahel rainfall

Permalink

<https://escholarship.org/uc/item/4w9030f2>

Journal

Climate Dynamics, 43(9-10)

ISSN

0930-7575

Authors

Liu, Yuwei
Chiang, John CH
Chou, Chia
[et al.](#)

Publication Date

2014-11-01

DOI

10.1007/s00382-014-2094-8

Peer reviewed

Atmospheric teleconnection mechanisms of extratropical North Atlantic SST influence on Sahel rainfall

Yuwei Liu

Department of Geography, University of California, Berkeley, California

John C. H. Chiang

Department of Geography and Center for Atmospheric Sciences,
University of California, Berkeley, California

Chia Chou

Research Center for Environmental Changes, Academia Sinica, and
Department of Atmospheric Sciences, National Taiwan University,
Taipei, Taiwan

Christina M. Patricola

Department of Atmospheric Sciences, Texas A&M University, College
Station, Texas

Corresponding Author:

Yuwei Liu

Department of Geography, University of California

531 McCone Hall, Berkeley, CA 94720

E-mail: yuwei2341@berkeley.edu

Tel: +15105022181

Abstract

1
2
3 Extratropical North Atlantic cooling has been tied to droughts over the Sahel in both
4 paleoclimate observations and modeling studies. This study, which uses an atmospheric
5 general circulation model (GCM) coupled to a slab ocean model that simulates this
6 connection, explores the hypothesis that the extratropical North Atlantic cooling causes
7 the Sahel droughts via an atmospheric teleconnection mediated by tropospheric cooling.
8 The drying is also produced in a regional climate model simulation of the Sahel when
9 reductions in air temperature (and associated geopotential height and humidity changes)
10 from the GCM simulation are imposed as the lateral boundary conditions. This latter
11 simulation explicitly demonstrates the central role of tropospheric cooling in mediating
12 the atmospheric teleconnection from extratropical North Atlantic cooling.

13 Diagnostic analyses are applied to the GCM simulation to infer teleconnection
14 mechanisms. An analysis of top of atmosphere radiative flux changes diagnosed with a
15 radiative kernel technique shows that extratropical North Atlantic cooling is augmented
16 by a positive low cloud feedback and advected downstream, cooling Europe and North
17 Africa. The cooling over North Africa is further amplified by a reduced greenhouse effect
18 from decreased atmospheric specific humidity. A moisture budget analysis shows that the
19 direct moisture effect and monsoon weakening, both tied to the ambient cooling and
20 resulting circulation changes, and feedbacks by vertical circulation and evaporation
21 augment the rainfall reduction. Cooling over the Tropical North Atlantic in response to
22 the prescribed extratropical cooling also augments the Sahel drying. Taken together, they
23 suggest a thermodynamic pathway for the teleconnection.

- 24 The teleconnection may also be applicable to understanding the North Atlantic
25 influence on Sahel rainfall over the 20th century.
- 26 Keywords: *North Atlantic cooling, Sahel, atmospheric teleconnection, monsoon*

27 1. Introduction

28 The Sahel region of Africa experienced megadroughts in both the recent and distant past.
29 Drought conditions periodically occurred throughout the late glacial period and the
30 Holocene, each event lasting from decades to several hundred years (Mulitza et al. 2008;
31 Shanahan et al. 2009). More recently, a severe Sahel drought occurred in the late
32 twentieth century, starting as an abrupt reduction in summer rainfall in the 1960's, and
33 lasting for over two decades with limited recovery to date (e.g. Nicholson 1979; Folland
34 et al. 1986). The megadroughts during the later stages of the last glacial period (~50,000
35 to 14,000 B.P.) have been tied to abrupt cold events over the North Atlantic (Wang et al.
36 2001; Mulitza et al. 2008; Shanahan et al. 2009; Niedermeyer et al. 2009; Stager et al.
37 2011). The link between North Atlantic cooling and African droughts persisted during the
38 Holocene, albeit at a weaker level (Shanahan et al. 2009).

39 Variation in the Atlantic meridional overturning circulation (AMOC) is thought
40 to be the leading cause of the North Atlantic abrupt climate changes. A slowdown of the
41 AMOC reduces the ocean heat transport into the North Atlantic, cooling the extratropical
42 North Atlantic in particular where the mean ocean heat transport convergence occurs.
43 This hypothesis was first proposed by Broecker et al. (1985), and subsequently supported
44 by many other studies (see Alley 2007 for a review). Moreover, simulations of the
45 AMOC slowdown in various coupled climate models (e.g. Vellinga and Wood 2002;
46 Zhang and Delworth 2005; Cheng et al. 2007; Chiang and Friedman 2012) all show
47 global climate impacts including a drying of the Sahel, similar to what is inferred from
48 paleodata (an example can be seen in Figure 5 of Chiang and Friedman 2012). Thus,

49 there is strong model evidence for a causal link between the North Atlantic cooling and
50 Sahel drought.

51 Previous studies have led to a hypothesis that atmospheric teleconnections of
52 extratropical North Atlantic cooling cause the impacts in the Sahel seen in AMOC
53 slowdown experiments (see Chiang and Friedman 2012 for a review). Motivation for this
54 hypothesis comes from the fact that an atmospheric general circulation model (AGCM)
55 coupled to a slab ocean, with cooling prescribed in the extratropical North Atlantic (50-
56 70°N) is able to produce very similar global climate changes as in AMOC slowdown
57 experiments. An example simulation using the Community Atmosphere Model 3-slab
58 ocean is shown in Fig. 1. (The simulation is described in detail in Chiang and Friedman
59 2012.) The simulation shows intense cooling over the extratropical North Atlantic that
60 extends over the whole Northern Hemisphere (NH), in particular to North Africa (Fig.
61 1a), and a strong rainfall reduction over the Sahel. A significant weakening of the
62 monsoon winds occurs over North Africa as indicated by the anomalous northeasterly
63 wind (Fig. 1b), co-incident with a meridional pressure gradient anomaly between the
64 anomalous high pressure to the north, and low pressure to the south. The model results
65 thus show a continental climate change primarily in temperature and sea level pressure
66 (SLP), which may act to bridge the extratropical North Atlantic cooling to the rainfall
67 reduction over the Sahel.

68 The mechanism for this atmospheric teleconnection is however still not known;
69 this is the focus of our study. Our approach is centered on the temperature and SLP
70 changes over the Sahara, north of the Sahel, that are apparent in the above simulations.
71 Previous studies support the idea that temperature and (consequently) SLP over North

72 Africa alters Sahel rainfall. Haarsma et al. (2005) found in observations that Sahel
73 rainfall was related to mean SLP over the Sahara, the latter in turn was related to surface
74 temperatures over North Africa. Biasutti et al. (2009) argued, based on lead-lag
75 correlation, that variation in the Sahara SLP caused variation in the Sahel rainfall. A
76 cursory examination of climate changes associated with Sahara temperature supports this
77 association: the left column of Fig. 2 shows the difference of precipitation, surface
78 temperature and SLP over the North Atlantic and North Africa for July to September
79 between the eight coldest and eight warmest periods in the Sahara since 1979. It shows
80 that a colder Sahara is accompanied by higher Sahara SLP and reduced Sahel rainfall
81 (and increased rainfall along the Guinea Coast). The cooling over the Sahara may weaken
82 the land-sea contrast and thus the monsoon flow. In addition, advection of air with low
83 moist static energy (MSE) limits the northward extent of the land convection zone by
84 displacing high MSE air that favors deep convection, a process known as the
85 “ventilation” mechanism (Chou et al. 2001). The intrusion of low MSE resulting from
86 cooling in the north may thus reduce rainfall over the Sahel. Taken together, these results
87 suggest that cooling in North Africa driven by extratropical North Atlantic cooling can
88 reduce the rainfall over the Sahel, possibly by weakening the land-sea thermal contrast
89 and reducing the MSE.

90 Our study analyzes the AGCM-slab ocean simulation which produces a reduction
91 in Sahel rainfall in response to prescribed extratropical North Atlantic cooling, with the
92 goal of developing a mechanistic view of this teleconnection. We hypothesize that the
93 North Atlantic influence is communicated to the Sahel through cooling air temperatures
94 over North Africa. We show the plausibility of our temperature hypothesis by showing

95 that the Sahel rainfall in a regional climate model (RCM) simulation is reduced when we
96 impose tropospheric cooling (and related geopotential height and humidity changes) in
97 the lateral boundary conditions of the model over the North African region. We then
98 apply various diagnostic analyses on the AGCM model simulation, including a moisture
99 budget analysis over West Africa. We also analyze radiative feedback and atmospheric
100 energy transport to determine how extratropical North Atlantic cooling is communicated
101 to lower latitudes. Ultimately, our goal is to understand how and why North Atlantic
102 stadials are linked to rainfall change over the Sahel during past climates, and also to see if
103 such mechanisms are applicable to today's climate.

104 In the next section, we describe the GCM and the RCM experiments and analysis
105 methods. This is followed by an analysis of the general climate response to extratropical
106 cooling in the GCM in Section 3. We then present results from the RCM in Section 4. In
107 section 5, we show how the North African cooling and extratropical North Atlantic
108 cooling are sustained from an energy budget perspective. The moisture budget of the
109 simulated Sahel rainfall response in the GCM is presented in Section 6. The results are
110 summarized and discussed in Section 7.

111 2. Experiments and methods

112 *a. Experiments*

113 We use the National Center for Atmospheric Research (NCAR) Community Atmosphere
114 Model version 3.5 (CAM3.5) coupled to a fixed-depth slab ocean model, which interacts
115 thermodynamically with the atmosphere, but has no representation of ocean dynamics
116 (Collins et al. 2006; Chen et al. 2010). The atmospheric model is configured with 26

117 vertical levels, and 64x128 horizontal grids. A monthly-varying ‘Q-flux’ is derived from
118 surface fluxes extracted from a fixed-SST simulation forced with global SST
119 climatology, and applied to the model slab. All greenhouse gas and aerosol forcings are
120 constant as present day values.

121 The slab ocean model is required, as the thermodynamic ocean-atmosphere
122 interaction is essential to communicating the extratropical influence to the tropics
123 (Chiang and Bitz 2005). We use the base configuration described above to undertake two
124 sets of simulations. In the first set, we replace the slab ocean in the North Atlantic over
125 the 45 °-60 °latitude band with climatological monthly-varying SSTs, and run this
126 configuration to equilibrium. In the second set, we also apply fixed SSTs over the same
127 North Atlantic region, but uniformly cool the applied SST by 2K. The applied cooling is
128 less than half of the typical estimates of extratropical North Atlantic SST changes from
129 interstadials to stadials (~4-6K, van Kreveld et al. 2000), but is sufficient to force a
130 significant reduction in Sahel rainfall (see Section 3). Both simulations are run for 60
131 years, and the climatology of the last 20 years is used for analysis. The difference
132 between the climatologies is used as the response to the extratropical cooling. The GCM
133 anomalies are shown as the July-August-September (JAS) average in the following
134 sections.

135 To explicitly show that the cooling over Sahara (and related low MSE) can drive a
136 Sahel rainfall decrease, we apply the cooling to the lateral boundary condition in a
137 regional model simulation of the Sahel. The regional model allows us to isolate the
138 impact of atmospheric cooling anomalies from the Sahara on the Sahel, enabling us to
139 directly test the hypothesis that extratropical North Atlantic cooling leads to Sahel rainfall

140 reduction through cooling the Sahara. We use the NCAR Weather Research and
141 Forecasting Model (WRF; Skamarock et al. 2008) version 3.3. It is a non-hydrostatic
142 model with 28 vertical levels, with the top of the atmosphere set to 50 hPa. The domain
143 chosen for the simulation is from 16.9 °W to 39.9 °E and from 30.7 °S to 29.3 °N,
144 incorporating the whole of Africa and in particular the Sahara.

145 The choice of horizontal resolution and physics options basically follows that of
146 the WRF simulation of North Africa by Patricola and Cook (2010). The horizontal
147 resolution used is 90 km, and the physics schemes are the Mellor-Yamada-Janjic
148 planetary boundary-layer scheme (Janjic 1994), the Monin-Obukhov Janjic surface-layer
149 scheme (Monin and Obukhov 1954; Janjic 1994; Janjic 1996; Janjic 2002), the Purdue
150 Lin microphysics scheme (Lin et al. 1983), and the RUC land-surface model (Smirnova
151 et al. 1997). Patricola and Cook (2010) showed that WRF with these options is able to
152 simulate a sufficiently accurate climatology over the Sahel. We use the Zhang-McFarlane
153 cumulus scheme (Zhang and Mcfarlane 1995), which differs from Patricola and Cook
154 (2010) but is the same convection scheme used in our CAM3.5 AGCM simulations. We
155 also use newer radiation schemes that are available in WRF version 3, the RRTMG
156 longwave and shortwave scheme (Mlawer et al. 1997). The simulation time step is 180
157 seconds.

158 The National Centers for Environmental Prediction (NCEP) –Department of
159 Energy (DOE) Atmospheric Model Intercomparison Project (AMIP-II) reanalysis (R-2)
160 6-hourly data (Kanamitsu et al. 2002) are used to specify the lateral boundary conditions
161 for the control simulation. Monthly temperature, geopotential height, and relative
162 humidity anomalies from the GCM runs are then added to the 6-hour reanalysis data for

163 the cooling simulation. The anomalies are added only at the northern boundary (and the
 164 relaxation zone) of the domain, since the purpose of the WRF simulation is to test our
 165 hypothesis that it is through modifying atmospheric temperature/energy over the Sahara
 166 that extratropical North Atlantic influences Sahel rainfall. Climatological skin
 167 temperature in the reanalysis data is used for SST. SST changes are not the focus of our
 168 study; and since the land makes up most of the domain, SST has little influence in our
 169 simulations. For both the control and cooling simulations, we conduct an ensemble of 10
 170 runs, starting from June 2 of each year from 2000 to 2009 and ending on September 2 of
 171 the following year. We run each simulation for fifteen months in order for the soil
 172 moisture to spin up, as soil moisture spin-up is important in the semi-arid Sahel region.
 173 The daily data from July and August of the following year are averaged as the summer
 174 climate. We averaged the ten summer climates separately for the control and cooling
 175 runs, and examined their differences.

176 *b. Diagnosis*

177 Two sets of diagnostic analyses are applied to the GCM simulation. In order to
 178 understand the communication of the cooling from the extratropical North Atlantic to
 179 other regions, we diagnose the atmospheric energy budget by examining both the top of
 180 atmosphere (TOA) energy flux and the atmospheric energy transport. We utilize a
 181 radiative kernel technique to separate changes of the TOA energy budget due to
 182 individual component changes (Soden et al. 2008):

$$183 \quad \delta R \approx \sum_i \frac{\partial R}{\partial X_i} \delta X_i, \quad (1)$$

184 where δR is the change in TOA energy flux, and terms inside the summation designate
 185 the change of R due to individual component X_i , including surface temperature T_s ,

186 atmospheric temperature T , water vapor q , surface albedo α , and clouds C . The
 187 differential $\partial R/\partial X_i$, which represents the change in TOA energy flux due to a unit change
 188 in each component, is the radiative kernel. Kernels for q and C are further split into
 189 shortwave (SW) and longwave (LW). We use radiative kernels calculated in CAM3
 190 (Shell et al. 2008; Soden et al. 2008) for all components but clouds. TOA energy flux
 191 change due to clouds is calculated as the adjusted cloud radiative forcing (CRF), defined
 192 as the difference between the TOA all-sky and clear-sky fluxes, with changes of CRF
 193 caused solely by non-cloud components removed (Shell et al. 2008). We also calculate
 194 the horizontal advection of MSE to examine how circulations adjust to balance the
 195 prescribed cooling and TOA radiative flux changes.

196 In order to understand the Sahel rainfall response to extratropical cooling, we
 197 diagnose the vertically integrated moisture budget equation as in Chou and Neelin (2004)
 198 and Chou et al. (2009) but with some modification:

$$199 \quad \delta P \approx - \langle \omega \frac{\partial \delta q}{\partial p} \rangle - \langle \mathbf{v} \cdot \nabla \delta q \rangle - \langle \delta \omega \frac{\partial q}{\partial p} \rangle + \langle \delta \mathbf{v} \cdot \nabla q \rangle + \delta E, \quad (2)$$

200 where $\langle . \rangle$ denotes vertical mass integration through the troposphere, and P , ω , q , p , E and
 201 \mathbf{v} denote precipitation, pressure velocity, specific humidity, pressure, evaporation, and
 202 horizontal velocity, respectively. The total rainfall change, δP , thus can be approximated
 203 by the summation of 1) anomalous vertical moisture transport associated with anomalous
 204 moisture δq , 2) anomalous horizontal moisture transport associated with anomalous
 205 moisture δq , 3) anomalous vertical moisture transport associated with anomalous vertical
 206 flow $\delta \omega$, 4) anomalous horizontal moisture transport associated with anomalous
 207 horizontal flow $\delta \mathbf{v}$ and 5) anomalous evaporation, as shown from left to right respectively
 208 in the right hand side (RHS) of the equation above.

209 3. Climate response to extratropical North Atlantic cooling

210 *a. Climate response over the Atlantic and North Africa*

211 Surface temperature and SLP are closely related to the Sahel rainfall in both observations
212 and model simulations (Haarsma et al. 2005; Biasutti et al. 2009; Liu and Chiang 2012);
213 therefore we begin presenting the GCM-simulated JAS averaged climate response to
214 extratropical North Atlantic cooling by showing those three fields (right column of Fig.
215 2). In the control run, the oceanic ITCZ is located north of the equator over the Atlantic,
216 extending into northeast Brazil and the west coast of the Sahel. Prescribed extratropical
217 North Atlantic cooling in turn leads to a cooling of the North Tropical Atlantic SST and a
218 southward displacement of the Atlantic ITCZ; these responses are well-known (e.g.
219 Chiang and Bitz 2005). Precipitation in the Sahel is reduced by over 25% in response to
220 the cooling, with a maximum anomaly of over 1 mm/day (Fig. 2d). Temperatures to the
221 north and west of the Sahel are colder, with a ~1K surface cooling across the midlatitude
222 Atlantic and Europe (Fig. 2e). The cooling south of 40 °N, though smaller, extends all the
223 way to near the equator over the ocean, and to the boundary between the Sahara and the
224 Sahel over North Africa. The maximum cooling over the Sahara is more than 0.5 K, and
225 located near the simulated heat low around 20 °N. Over the Sahel, temperatures are
226 warmer in association with reduced rainfall, which supports a reduced evaporative
227 cooling and increased solar radiation at the surface.

228 SLP over the Sahara is also increased in association with the North Atlantic
229 cooling (Fig. 2f); this response is likely causally linked to the cooling (discussed later).
230 The pressure increase over North Africa peaks near the climatological Sahara Low with a
231 magnitude of ~1 hPa, leading to decreased meridional SLP contrast between the Sahara

232 and the Gulf of Guinea. Overall, a broad cooling and coincident SLP increase appear over
233 the Atlantic and North Africa, and rainfall is reduced over the Sahel with a slight increase
234 over the Guinean Coast, consistent with results from previous studies on extratropical
235 North Atlantic cooling (e.g. Mulitza et al. 2008; Liu and Chiang 2012). The simulated
236 response in North African climate to extratropical North Atlantic cooling resembles the
237 observed difference of climate in cold and warm Sahara periods (left column of Fig. 2),
238 lending confidence to our hypothesis that temperature over the Sahara broadcasts the
239 extratropical signal to the Sahel.

240 Extratropical North Atlantic SST cooling induces changes in atmospheric
241 temperature, specific humidity, and clouds, which exert feedbacks to the initial
242 temperature change by altering the TOA energy budget. We present these changes of in
243 Fig. 3. Mean tropospheric temperature, defined as the mass-weighted vertical average of
244 atmospheric temperature from the surface to 100mb, broadly decreases in the domain
245 (Fig. 3a). Mean tropospheric specific humidity, calculated similarly to mean tropospheric
246 temperature, decreases in response to the cooling (Fig. 3b), following the Clausius–
247 Clapeyron relation in regions where relative humidity varies little, especially north of the
248 Sahel. The drop in humidity appears to peak over convective regions, in particular in the
249 Sahel where mean tropospheric humidity is reduced by about 0.3 g/kg; this is consistent
250 with the reduction in convection there. Changes in both mean tropospheric temperature
251 and humidity (and also geopotential height which is small, not shown) result in a
252 substantial decrease in MSE (Fig. 3c), with two maxima corresponding to the maximum
253 change of temperature in the extratropics, and of humidity in the Sahel.

254 In the extratropics, cooler SST over the North Atlantic favors boundary layer
255 inversions, leading to an increase in low clouds (surface to 700 mb, Fig. 3d). In the
256 tropics, low clouds decrease over the Sahel in association with the reduction in
257 convection. High clouds (400mb to the model top) decrease over both the northern ocean
258 and the Sahel and increase over the southern edge of climatological ITCZ and northeast
259 Brazil, in accordance with the rainfall change (Fig. 3e). The change in middle clouds
260 (700 mb to 400 mb) generally follows that of low clouds except for a slight decrease over
261 the extratropical North Atlantic (not shown).

262 *b. Vertical profile of climate anomalies over North Africa*

263 The GCM-simulated Sahelian rainfall reduction in response to extratropical North
264 Atlantic cooling largely results from anomalous convection and monsoonal flow. We
265 present vertical profiles of the circulation, temperature and humidity anomalies from the
266 cooling minus control GCM simulations to illustrate this point (Fig. 4). All fields are
267 averaged between 10 °W and 30 °E. Substantial cooling reaches 20 °N, with a maximum of
268 more than 0.7K in the middle troposphere (Fig. 4a). The strong cooling over the Sahara
269 results in a meridional temperature gradient anomaly. Over the Sahel between 10 °N and
270 20 °N, a vertical dipole is seen with warming near the surface and cooling in the middle
271 and upper troposphere. The dipole is likely a consequence of the increase in the Bowen
272 ratio at the surface and the suppression of deep convection; combined, they lead to less
273 water vapor being evaporated into the atmosphere from the surface and brought to the
274 middle troposphere for condensation, while more heat warms the lower troposphere in
275 the form of sensible heat. The specific humidity is reduced considerably over North
276 Africa and the reduction is largely confined to the lower troposphere, consistent with the

277 reduction of convection there (Fig. 4b). The magnitude of change generally reaches 0.3
278 g/kg, and can exceed 0.5 g/kg in the lower troposphere over the Sahel.

279 The vertical wind anomaly shows a 20% increase in subsidence north of the Sahel
280 and a decrease in ascent over the Sahel (Fig. 4c). The substantial sinking anomaly near
281 the climatological subsidence zone over the Sahara acts to balance the cooling through
282 adiabatic compression. Over the Sahel, there is a dipole with enhanced (weakened) uplift
283 below (above) 800mb, indicating decreased deep convection and a slight enhancement of
284 shallow thermal convection.

285 The upper level tropical easterly jet (TEJ) at 200mb, with a climatological core
286 around 10 °N, induces upper level divergence and thus lower level convergence and
287 convection (Nicholson 2009). In the experiment, the TEJ is weakened in response to the
288 negative temperature gradient (Fig. 4d), similar to the observed circulation change in
289 Sahel dry years as found by Nicholson (2009).

290 The mid-level African easterly jet (AEJ) is only vaguely simulated at 600mb
291 around 17 °N in the control run. A strong easterly anomaly, however, appears at 12 °N
292 between 500mb and 800mb in the experiment, suggesting a southward shift and
293 strengthening of the AEJ. The easterly anomaly is likely caused by the positive
294 temperature gradient as a result of the low-level warming between 10 °N and 20 °N (Fig.
295 4a). Grist and Nicholson (2001) found in observations that the AEJ induces cyclonic
296 (anticyclonic) shear to its south (north) and that a southward AEJ shift likely displaces
297 the rainbelt southward, thus reducing the rainfall over the Sahel. Cook (1999) and
298 Patricola and Cook (2008) found that changes in the AEJ, which depend on the
299 meridional temperature/soil moisture gradients, can also reduce rainfall by transporting

300 moisture away from the Sahel. Therefore, a positive feedback exists in our simulation: as
301 a rainfall decrease reduces soil moisture and thus leads to surface warming, a consequent
302 positive temperature gradient in the low level strengthens the AEJ and displaces it
303 southward, which in turn further reduces rainfall over the Sahel.

304 The southwesterly monsoon flow, which extends to 800mb climatologically, is
305 weakened by up to 30% in the lower troposphere (Fig. 4d and 4e), probably due to the
306 diminished meridional temperature/pressure gradient. Climatological northerlies from the
307 Sahara converge with the monsoon flow over the Sahel. The strengthened northerlies in
308 the cooling simulation bring anomalously dry and cool air to the Sahel, weakening the
309 low-level convergence and shifting it southward.

310 4. Testing the temperature hypothesis using a WRF 311 simulation of the Sahel

312 While the GCM-modeled Sahel climate response is consistent with the influence of
313 atmospheric and surface cooling over the Sahara, it does not demonstrate causality. We
314 explicitly show that the cooling can drive a rainfall decrease over the Sahel, by applying
315 temperature, humidity, and geopotential height anomalies as exterior boundary condition
316 in a WRF simulation of the Sahel. With those GCM anomalies applied only to the
317 northern boundary of the RCM domain, the WRF simulation produces a response in
318 Sahel climate to Sahara tropospheric cooling comparable to the response in Sahel climate
319 to extratropical North Atlantic cooling in the GCM. The simulated precipitation anomaly
320 (Fig. 5a) exhibits finer structures due to the higher resolution of the WRF model, but the
321 overall change resembles that in the GCM. Drying with a maximum of over 1 mm/day

322 appears between 10 °N and 20 °N over North Africa; both the location and magnitude of
323 this drying are comparable to the GCM response (Fig. 2d). Scattered drying and wetting
324 are shown south of the Sahel in WRF, leading to a neutral or slightly positive overall
325 precipitation change as in the GCM. The overall precipitation change, in particular the
326 substantial decrease in the Sahel, suggests a retreat of the monsoon convection, consistent
327 with the ventilation mechanism where low MSE from the north limits the extent of land
328 convection. Precipitation north of 10 °N along the west coast, which is influenced by the
329 oceanic ITCZ (Fig. 2d), exhibits little change, as change in SST is not taken into account
330 in the WRF simulation.

331 The regional model also reproduces the surface temperature and pressure response
332 to atmospheric cooling (Fig. 5b and 5c) with magnitudes comparable to those in the
333 GCM experiment. Cooling spreads from the northern boundary of the domain to the
334 vicinity of Sahel, where the surface warms as a result of the rainfall reduction. As WRF
335 does not output SLP, we take surface pressure instead for comparison. The surface
336 pressure in WRF (Fig. 5c), similar to the SLP in the GCM (Fig. 2f), increases over the
337 Sahara, reducing the strength of the Sahara Low and thus the pressure gradient between
338 North Africa and the tropical Atlantic.

339 Vertical profiles of the WRF-simulated wind anomalies, averaged from 10 °W to
340 30 °E are shown in Fig. 5 (compare to the GCM fields in figure 4). The WRF responses to
341 prescribed anomalies relevant to cooling on the northern lateral boundary condition are
342 largely comparable to those of the GCM simulation, except that since the mean Sahel
343 uplift region is located somewhat north (~20 °N) of the GCM uplift region (~17 °N), the
344 WRF anomalies are similarly shifted. The sinking anomaly north of 20 °N and the vertical

345 dipole over the Sahel are apparent in WRF simulation (Fig. 5d), although the near-surface
346 uplift anomaly south of 20°N looks deeper in WRF than in the GCM. The response of the
347 zonal wind (Fig. 5e) in the upper troposphere, which basically follows the thermal wind,
348 is identical with that in CAM (Fig. 4d). However, unlike the anomalous low-level
349 northerlies south of 30°N in the GCM, WRF exhibits anomalous low-level northerlies
350 from 15°N-30°N, and anomalous low-level southerlies to the south of 15°N (compare
351 Fig. 5f and 4e). As a consequence, there is a slight southward shift of the low-level
352 convergence center toward the Guinea Coast, bringing about the anomalous low-level
353 convergence around 18°N and compensating divergence around the 600mb level. The
354 shifted convergence is weaker and the convection is shallower in the cooling simulation
355 compared with the climatology, consistent with the reduction in rainfall.

356 Differences in details aside, anomalies relevant to cooling from CAM3.5 forced
357 only at the northern lateral boundary of the WRF domain generally simulate the Sahel
358 rainfall reduction and associated temperature, pressure, and circulation changes as in the
359 GCM experiment which is forced with extratropical North Atlantic SST cooling. Our
360 WRF simulation thus provides strong evidence that the Sahel rainfall changes in the
361 GCM experiment result from large-scale cooling in tropospheric temperatures north of
362 the Sahel.

363 5. How is the cooling communicated and maintained?

364 Cooling over the Sahara is key to our proposed teleconnection. It then begs the question
365 of how the temperature changes are communicated from the high-latitude North Atlantic.
366 We have shown that the prescribed 2K SST cooling in the extratropical North Atlantic
367 causes significant cooling in the Atlantic sector, with a magnitude generally larger than

368 1K in the midlatitude Atlantic and Europe, and as much as 0.5K near the Sahel. How is
369 such a strong cooling response maintained both near and far from the source?

370 We first explore this question by evaluating the radiative feedbacks that help
371 amplify and maintain the cooling far from its source region. TOA radiative flux
372 anomalies in response to the North Atlantic cooling in the GCM simulations are shown in
373 Fig. 6, separated into contributions by cloud, moisture, and temperature changes
374 (downward is positive, so negative values mean energy loss and thus more cooling of the
375 atmosphere, acting as a positive feedback). As shown in Fig. 3, a sizable increase of low
376 clouds, presumably stratus, appears over the ocean in association with prescribed cooling;
377 this is likely due to the surface-cooling induced boundary layer inversion. The stratus
378 cloud cover exerts a strong positive feedback by reflecting more SW than it absorbs LW
379 (Fig. 6a and 6c). This cooling effect dominates in the extratropics. On the other hand,
380 cloud cover decreases over North Africa, in particular over the Sahel, consistent with the
381 reduced convection there. Reduced cloud cover allows for more incoming SW to the
382 atmosphere but also leads to more outgoing longwave radiation (OLR) (Fig. 6a and 6c).
383 The two competing effects largely cancel, leaving a slight SW gain over the Sahel, which
384 partially contributes to the surface warming. Overall, cloud feedbacks are positive and
385 dominant in extratropics, but relatively weak in tropics (Fig. 6e).

386 A negative LW flux anomaly due to reduced tropospheric humidity appears across
387 the North Atlantic and into Europe and North Africa (Fig. 6b), leading to a considerable
388 increase in clear-sky OLR, a major positive radiative feedback in tropics. Water vapor is
389 also a SW absorber and thus contributes to a small positive feedback to cooling from
390 reducing shortwave absorption (not shown). Maximum cooling from the LW moisture

391 feedback is collocated over the Sahel with the maximum of water vapor reduction.
 392 Another positive feedback involves the surface albedo change (not shown), as the
 393 brighter surface reflects SW as more ice forms in high latitudes. Decreased incoming SW
 394 due to albedo is also found over the Sahel, with a smaller magnitude than that in high
 395 latitudes.

396 Taken together, total clouds, moisture, and surface albedo yield an overall
 397 positive feedback in the Atlantic sector, as well as over North Africa (Fig. 6f). In
 398 particular, the positive SW cloud feedback dominates in the extratropics whereas the
 399 positive LW moisture feedback prevails in the tropics. All the positive feedbacks lead to
 400 further energy loss in addition to the prescribed cooling, and such energy loss requires a
 401 decrease in surface and tropospheric temperature and change in lapse rate to compensate
 402 by reducing OLR (Fig. 6d).

403 To better quantify the significance of the cloud and water vapor feedback on
 404 enhancing atmospheric cooling, we estimate the atmospheric temperature anomalies
 405 associated with those feedbacks. We start with the vertically integrated energy budget,
 406 which, in equilibrium, is

$$407 \quad 0 = \delta F_A + \delta F_s + \delta R, \quad (3)$$

408 where δF_A is anomalous horizontal heat convergence, δF_s is anomalous surface flux into
 409 the atmosphere (which is nonzero over the extratropical North Atlantic in our
 410 simulation), and δR is the change in TOA energy flux. Expanding δR as in equation (1),
 411 and rearranging the above equation give

$$412 \quad \delta T = -\frac{1}{\frac{\partial R}{\partial T}} (\delta R_c + \delta R_{wlw} + \delta R_{rest} + \delta F_A + \delta F_s). \quad (4)$$

413 The first three terms in the parentheses on the RHS are the TOA energy flux
414 anomalies related to total cloud feedback, δR_c , LW water vapor feedback, δR_{wlw} , and all
415 other feedbacks, δR_{rest} , respectively. Each energy flux anomaly in the parentheses is
416 divided by the vertical integral of the air temperature kernel, $\partial R/\partial T$, to yield the partial
417 temperature change of a “slab” atmosphere due to the anomaly. We present the first two
418 terms on the RHS of equation (4), partial temperature changes due to clouds and water
419 vapor, in Fig. 6g and 6h. As the spatial variance of the temperature kernel is small (not
420 shown), the spatial pattern of the feedback-derived air temperature change generally
421 follows the TOA flux anomalies, but the magnitude is three times as large as the
422 simulated mean tropospheric temperature anomaly (Fig. 3a). The temperature decrease
423 due to cloud feedbacks is over 2K in most of the extratropical North Atlantic, with a
424 maximum of over 4K; whereas the maximum modeled mean tropospheric temperature
425 cooling is ~ 1 K; the water vapor feedback dominates in the tropics, in particular over
426 North Africa, and the consequent partial temperature change is slightly larger than that in
427 the simulation.

428 We now examine how the energy transport by the atmospheric circulation adjusts
429 to balance the TOA radiative flux changes. We calculate the change in the horizontal
430 advection of MSE (Fig. 7a), decomposed into contributions by anomalous MSE
431 advection by the climatological flow (Fig. 7b), and advection of climatological MSE by
432 the anomalous flow (Fig. 7c). The residual, mainly consisting of the non-linear term, is
433 small and thus neglected. Overall, horizontal MSE advection propagates cooling from the
434 extratropical North Atlantic downstream - to Europe, the subtropical North Atlantic, and
435 North Africa (Fig. 7a). The magnitude much larger than that of the radiative feedbacks.

436 The low MSE advection is completed mainly by the climatological westerlies in the
437 extratropics (Fig. 7b), and by anomalous northely flow over North Africa (Fig. 7c). The
438 advection further decomposed into contributions from each component of MSE, reveals
439 that over the Sahara the cooling is induced by cold air invasion, while in the Sahel it is
440 caused by decreased latent heat energy input from weakened monsoon flow (not shown).

441 Intrusion of air with low moist static energy (MSE) to the subtropics limits the
442 poleward extent of the continental convergence zone by displacing high MSE air that
443 favors deep convection, a mechanism known as ventilation (Chou *et al.* 2001). If the
444 advection of low MSE air into North Africa is indeed the mechanism for the Sahel
445 rainfall reduction, can the Tropical North Atlantic – which also cools in response to
446 imposed extratropical North Atlantic cooling – act to augment drying over the Sahel? In
447 order to test this, we perform two idealized simulations: in the first, we apply
448 extratropical North Atlantic cooling but keep the Tropical North Atlantic SST fixed to the
449 climatology (by replacing the slab ocean there with prescribed SST); in the second, we
450 prescribe SST cooling only over the Tropical North Atlantic at the same level as in the
451 ‘usual’ slab-ocean simulation with extratropical North Atlantic cooling. Thus, the first
452 simulation tests the teleconnection without the Tropical North Atlantic SST feedback,
453 and the second is the feedback contribution. The results (figures not shown) show that the
454 Tropical North Atlantic SST feedback does indeed augment the Sahel drying, but the
455 majority (over two thirds) of the drying is achieved without this feedback. This result is
456 consistent with the ventilation argument, as the westerlies are stronger in the midlatitudes
457 whereas in the tropics the climatological flow is easterly.

458 In summary, radiative feedbacks, tropical SST feedbacks, and atmospheric
459 transport cooperate to communicate extratropical cooling to the Sahel. Extratropical
460 North Atlantic cooling - augmented by a positive low cloud feedback - is advected
461 downstream by the climatological midlatitude westerlies, cooling Europe and North
462 Africa. Circulation changes over North Africa further reduce the MSE, by importing cold
463 air and countering the advection of latent heat energy from the monsoon flow. Cooling
464 over North Africa is further amplified by a reduced greenhouse effect from decreased
465 atmospheric specific humidity. Finally, a cooler Tropical North Atlantic also acts to
466 augment drying over the Sahel.

467 6. Moisture budget analysis of the Sahel rainfall response

468 Our results thus far point strongly to cooling north of the Sahel as the cause of the Sahel
469 rainfall change. In this section we diagnose the moisture budget over the Sahel in the
470 GCM simulation, to infer how the rainfall changes are linked to the cooling.

471 *a. Moisture budget analysis*

472 Fig. 8 shows each term of the vertically-integrated moisture budget from the RHS of
473 equation (2) (note these terms, factoring in the latent heat of vaporization, are plotted in
474 energy units, W m^{-2}). Changes in specific humidity contribute considerably to the
475 reduction of rainfall over the Sahel (Fig. 8a and 8b), and its effect is mainly through
476 vertical transport anomalies. Humidity decreases primarily in the lower troposphere,
477 resulting in a negative vertical moisture gradient anomaly (Fig. 4b). Therefore over the
478 Sahel (a region of mean ascending motion) this term leads to drying (Fig. 8a). The
479 reverse effect - that a weakened vertical humidity gradient makes the downward transport

480 less arid - holds for subsidence regions of the Sahara. The humidity exhibits a positive
481 meridional gradient anomaly over North Africa, as the Sahel dries out more than the
482 Sahara (Fig. 3b). With the climatological wind being northerly at the boundary between
483 the Sahara and Sahel, the humidity anomaly wets the transition zone (Fig. 8b).

484 The term of the largest magnitude on the RHS of equation (2) is the anomalous
485 vertical moisture transport caused by the sinking anomaly (Fig. 8c). The dipole at the
486 very western edge of the Sahel with a negative anomaly in the north and positive
487 anomaly in the south marks the southward shift of the Atlantic marine ITCZ. Further
488 inland, such a dipole-like signature is only seen in Central and East Africa, with the rest
489 of the area being dominated by near-uniform drying.

490 Reduced horizontal moisture transport by changes in the horizontal winds
491 contributes significantly to the local rainfall reduction over central Sahel (Fig. 8d). This is
492 mainly due to a reduction of the southerly flow, as demonstrated in a further split of this
493 term into contributions from zonal and meridional wind (not shown). Evaporation
494 decreases between 15 °N and 20 °N (Fig. 8e), primarily in association with the reduced
495 soil moisture; warmer temperatures here would tend to increase evaporation, but
496 evaporation over the Sahel semi-arid region is moisture- rather than temperature-limited.
497 This is in contrast to West Africa along 10 °N, where surface warming actually increases
498 evaporation.

499 ***b. Processes of the Sahel rainfall reduction***

500 Three major processes of the Sahel rainfall reduction are suggested from the above
501 analysis. The first is the “direct moisture effect”, the change in vertical moisture transport
502 due to anomalous specific humidity. This effect has been proposed previously by Chou

503 and Neelin (2004) to explain the tropical precipitation response to global warming; they
504 demonstrated that an increase in gross moisture stratification due to low-level moisture
505 increases with global warming leads to increased rainfall in climatological convergence
506 regions, as part of the rich-get-richer mechanism. In our cooling simulation, the direct
507 moisture effect acts in the opposite way by decreasing rainfall in convective regions, or
508 rich-get-poor (Fig. 8a). The decrease in specific humidity comes about partly due to the
509 tropospheric cooling in vicinity of the Sahel that makes the atmosphere hold less
510 moisture, and partly as a result of circulation changes.

511 The second process, the change in the vertical moisture transport due to
512 anomalous vertical wind, also contributes significantly to Sahel rainfall reduction. This
513 term is a dynamic feedback associated with a reduction of low-level moisture content
514 (Chou and Neeling 2004). An analysis of the local MSE budget (not shown) following
515 Chou and Neelin (2004) reveals both an increase of moist stability due to drying and an
516 increase of dry instability due to low-level warming. The former overtakes the latter,
517 resulting to a more stable atmosphere, consistent with the weakened convection.

518 The third process is related to the monsoon flow. Cooling over the Sahara reduces
519 the land-sea contrast in the West African monsoon regime, leading to a positive pressure
520 anomaly in the Sahara and a weakening of the meridional pressure gradient (Fig. 2f). The
521 southwesterly monsoon flow carrying moisture inland from the Gulf of Guinea is reduced
522 accordingly, while dry air advection from the Sahara to the Sahel increases (Fig 4e);
523 these lead to the moisture transport changes due to anomalous horizontal wind seen in
524 Fig. 8d.

525 In addition to the three main processes, reduced evaporation over the Sahel plays
526 a significant role in reducing rainfall. This presumably arises from a soil-moisture
527 feedback – a positive feedback loop is set up once decreased precipitation reduces soil
528 moisture, which in turn weakens evaporation and thus lower-tropospheric moisture
529 available for precipitation. The evaporation effect is more restricted to the northern part
530 of the rainfall reduction, presumably because soil moisture is a greater limiting factor for
531 precipitation close to the Sahel-Sahara transition. On the other hand, toward the Guinea
532 Coast the increased evaporation tends to enhance rainfall.

533 Taken together, the Sahel rainfall reduction is associated with reduced specific
534 humidity, reduced vertical flow and weaker monsoon flow, and reduced local
535 evaporation. Those changes are consistent with the decreased land-sea contrast created by
536 the cooling and consequent circulation change, and dynamic/thermodynamic feedbacks
537 of the two. However, given that the moisture budget is a diagnostic analysis, no causal
538 relationship should be drawn from the results before further mechanistic study is done.

539 7. Concluding notes

540 *a. Conclusion*

541 We investigate teleconnection mechanisms of how extratropical North Atlantic cooling
542 reduces summertime rainfall over the Sahel, using simulations of atmospheric general
543 circulation model (the NCAR Community Atmosphere Model version 3.5, CAM3.5)
544 coupled with a slab ocean. The hypothesis we propose is that the extratropical North
545 Atlantic influence is communicated to the Sahel through air temperatures over North
546 Africa, and that the Sahel rainfall is a direct response to the temperatures. Forced by 2K

547 cooling in extratropical North Atlantic SST, the AGCM simulates surface cooling which
548 spreads throughout the North Atlantic and surrounding continents, and penetrates into the
549 Sahara (Fig. 2e). Rainfall decreased by more than 25% in the semi-arid Sahel area
550 between 10 °N and 20 °N across Africa (Fig. 2d). Other climate signatures are linked to
551 the cooling, including a low cloud cover increase in the extratropics (Fig. 3d), SLP
552 increase (Fig. 2f) and humidity and MSE decrease (Fig. 3b and 3c) north of the Sahel,
553 enhanced subsidence over the Sahara, and weakened upper level easterly jet and low
554 level monsoon flow over the Sahel (Fig. 4).

555 We then use a regional model – the Weather Research and Forecasting (WRF)
556 model – to explicitly show that cold air anomalies over the Sahara can drive rainfall
557 decreases over the Sahel. We apply cooling and related decreased geopotential height and
558 humidity forcings derived from the GCM simulation as the northern lateral boundary
559 condition in the WRF model, whose domain is set over Africa; the resulting changes to
560 the Sahel rainfall and North African climate were broadly similar to the GCM response
561 (Fig. 5). Our WRF simulation thus strongly bolsters our hypothesis that the Sahel rainfall
562 changes in the GCM forced with extratropical North Atlantic cooling result from large-
563 scale cooling to the tropospheric temperatures north of the Sahel.

564 Our analysis suggests that the teleconnection is mediated by the advection of
565 anomalously cold, dry air from the extratropical North Atlantic to North Africa (Fig. 7).
566 Climatological midlatitude westerlies bring low MSE air from the extratropics to North
567 Africa, where the MSE is further reduced by increased (decreased) import of cold (wet)
568 air by anomalous northerlies. This ventilation effect removes heat from land and thus
569 hinders convection, as shown in Chou et al. (2001). We also find that the Tropical North

570 Atlantic, which also cools in response to the extratropical North Atlantic cooling,
571 augments the Sahel drying; but this feedback response is relatively small.

572 We find that radiative feedbacks also augment the teleconnection. A radiative
573 kernel (Shell et al. 2008; Soden et al. 2008) analysis on our simulation show that the
574 positive cloud shortwave feedback considerably enhances the cooling in the extratropics,
575 in particular over the North Atlantic, while positive moisture longwave feedbacks
576 dominates in the tropics (Fig. 6). It suggests that these feedbacks are able to leverage the
577 effects of extratropical North Atlantic cooling: specifically, increased low clouds form
578 over the extratropical North Atlantic in response to the imposed surface cooling could
579 have led to over a 2K uniform drop in atmospheric temperature, if no negative feedback
580 or horizontal heat convergence were present (Fig. 6g); Decreases in tropospheric specific
581 humidity reduce the associated greenhouse effect – this cooling is specifically effective in
582 acting remotely from the North Atlantic (Fig. 6h).

583 Finally, we analyze the vertically-integrated moisture budget over the Sahel,
584 following Chou and Neelin (2004) and Chou et al. (2009), to explore the link between the
585 contiguous cooling and the Sahel rainfall response. The decreased Sahel rainfall was
586 primarily balanced by the direct moisture effect, stability increase, and monsoon
587 weakening, processes that were tied to the ambient cooling and resulting circulation
588 changes (Fig. 8). Positive feedbacks between soil moisture and precipitation also
589 contributed to the rainfall reduction. These analyses explicitly link the rainfall reduction
590 to the cooling, but do not assign causality.

591 Our analysis demonstrates the plausibility of the atmosphere-mediated mechanism
592 for the propagation of cooling, and the key factors in maintaining the teleconnection once

593 it is set up. However, more work is required to develop and test the teleconnection
594 mechanism. An examination of the evolution of transient radiative feedbacks,
595 atmospheric circulation and related energy transport, and the interaction of the two after
596 the onset of the extratropical North Atlantic cooling, would be useful in this regard.

597 ***b. Relevance to the 20th century Sahel Drought***

598 The proposed teleconnection mechanism may be relevant to the recent Sahel
599 drought that occurred in the late 1960's (e.g. Nicholson 1979; Folland et al. 1986).
600 Various sources including greenhouse gases, anthropogenic aerosols, SSTs, and local
601 land changes are linked to the Sahel drought (e.g. Folland et al. 1986; Folland et al. 1991;
602 Xue and Jagadish 1993; Rowell et al. 1995; Fontaine et al. 1998; Rotstayn and Lohmann
603 2002; Bader and Latif 2003; Giannini et al. 2003; Biasutti and Giannini 2006; Held et al.
604 2006; Hoerling et al. 2006; Zhou et al. 2008; Kawase et al. 2010; Liu and Chiang 2012),
605 among which SSTs, in particular over the Atlantic, have been shown to play a key role.
606 Folland et al. (1986) showed that the onset of the Sahel drought was tied to an
607 interhemispheric SST gradient with cooling in the Northern Hemisphere and warming in
608 the Southern Hemisphere, particularly in the Atlantic. Apart from the gradient, a striking
609 feature related to the drought is intense cooling in high-latitude North Atlantic. The effect
610 of this SST pattern in drying the Sahel has been confirmed in subsequent studies (Folland
611 et al. 1991; Rowell et al. 1995; Fontaine et al. 1998). Liu and Chiang (2012) specifically
612 showed that the Sahel drought is tied to cooling over Eurasia and North Africa, and both
613 the drought and cooling are a consistent climate signature with the observed extratropical
614 North Atlantic SST drop in the late 1960's. This linkage suggests that the paleo-scenario
615 that extratropical North Atlantic cooling leads to a Sahel rainfall reduction also applies to

616 the twentieth century. The current study may shed light on the mechanism of
617 teleconnection from the North Atlantic to the Sahel in modern climate.

618

619 8. Acknowledgements

620 This research is supported by the National Science Foundation (NSF AGS-1143329 and
621 NSF EAR-0909195). The authors would like to thank Inez Fung, Shih-Yu Lee, Andrew
622 Friedman and Ching-Yee Chang for useful and enlightening discussions. YL thanks
623 Ivana Cvijanovic for helping design the GCM simulation, Alexandra Jonko for assistance
624 with using the radiative kernel technique, Andrew Friedman and Meghan Thurlow for
625 editing the manuscript for grammar and usage. All reanalysis data are provided by the
626 NOAA/OAR/ESRL PSD, Boulder, Colorado, USA, at <http://www.esrl.noaa.gov/psd/>.

627 9. References

- 628 Adler RF, Huffman GJ, Chang A, et al. (2003) The version-2 global precipitation
629 climatology project (GPCP) monthly precipitation analysis (1979-present). J
630 Hydrometeorol 4:1147-1167. doi: 10.1175/1525-
631 7541(2003)004<1147:TVGPCP>2.0.CO;2
- 632 Alley RB (2007) Wally was right: Predictive ability of the North Atlantic “conveyor belt”
633 hypothesis for abrupt climate change. Annu Rev Earth Planet Sci 35:241–272.
- 634 Bader J, Latif M (2003) The impact of decadal-scale Indian Ocean sea surface
635 temperature anomalies on Sahelian rainfall and the North Atlantic Oscillation.
636 Geophys Res Lett 30:2169.

- 637 Biasutti, M, Giannini, A. (2006). Robust Sahel drying in response to late 20th century
638 forcings. *Geophys Res Lett*, 33(11).
- 639 Biasutti M, Sobel A, Camargo S (2009) The Role of the Sahara Low in Summertime
640 Sahel Rainfall Variability and Change in the CMIP3 Models. *J Clim* 22:5755–5771.
641 doi: 10.1175/2009JCLI2969.1
- 642 Broecker WS, Peteet DM, Rind D (1985) Does the ocean-atmosphere system have more
643 than one stable mode of operation? *Nature* 315:21–26. doi: 10.1038/315021a0
- 644 Chen, H, Zhou T, Neale R, Wu X, Zhang G (2010) Performance of the new NCAR
645 CAM3. 5 in East Asian summer monsoon simulations: Sensitivity to modifications of
646 the convection scheme. *J Clim*, 23:3657–3675.
- 647 Cheng W, Bitz CM, Chiang JCH (2007) Adjustment of the global climate to an abrupt
648 slowdown of the Atlantic meridional overturning circulation. *Geophys Monogr*,
649 173:295.
- 650 Chiang JCH, Bitz CM (2005) Influence of high latitude ice cover on the marine
651 Intertropical Convergence Zone. *Clim Dyn* 25:477–496.
- 652 Chiang JCH, Friedman AR (2012) Extratropical Cooling, Interhemispheric Thermal
653 Gradients, and Tropical Climate Change. *Annu Rev Earth Planet Sci Vol* 40 40:383–
654 412.
- 655 Chou C, Neelin J, Su H (2001) Ocean-atmosphere-land feedbacks in an idealized
656 monsoon. *Q J R Meteorol Soc* 127:1869–1891. doi: 10.1002/qj.49712757602
- 657 Chou C, Neelin JD (2004) Mechanisms of global warming impacts on regional tropical
658 precipitation. *J Clim* 17:2688–2701. doi: 10.1175/1520-
659 0442(2004)017<2688:MOGWIO>2.0.CO;2

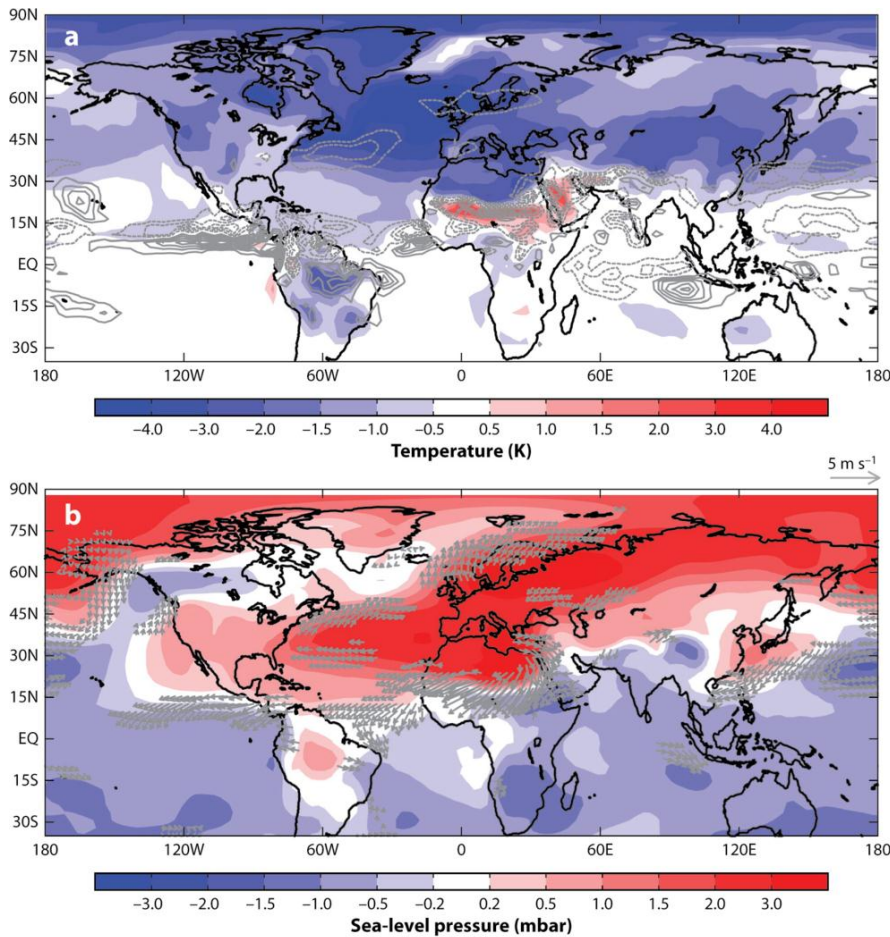
- 660 Chou C, Neelin JD, Chen C-A, Tu J-Y (2009) Evaluating the "Rich-Get-Richer"
661 Mechanism in Tropical Precipitation Change under Global Warming. *J Clim*
662 22:1982–2005. doi: 10.1175/2008JCLI2471.1
- 663 Collins W, Rasch P, Boville B, et al. (2006) The formulation and atmospheric simulation
664 of the Community Atmosphere Model version 3 (CAM3). *J Clim* 19:2144–2161.
- 665 Cook K (1999) Generation of the African easterly jet and its role in determining West
666 African precipitation RID B-4998-2011. *J Clim* 12:1165–1184. doi: 10.1175/1520-
667 0442(1999)012<1165:GOTAEJ>2.0.CO;2
- 668 Folland CK, Owen J, Ward MN, Colman A (1991) Prediction of seasonal rainfall in the
669 sahel region using empirical and dynamic methods. *J Forecast* 10:21–56. doi:
670 10.1002/for.3980100104
- 671 Folland CK, Palmer TN, Parker DE (1986) Sahel Rainfall and Worldwide Sea
672 Temperatures, 1901-85. *Nature* 320:602–607.
- 673 Fontaine B, Trzaska S, Janicot S (1998) Evolution of the relationship between near global
674 and Atlantic SST modes and the rainy season in west Africa: statistical analyses and
675 sensitivity experiments. *Clim Dyn* 14:353–368. doi: 10.1007/s003820050228
- 676 Giannini A, Saravanan R, Chang P (2003) Oceanic forcing of Sahel rainfall on
677 interannual to interdecadal time scales. *Science* 302:1027–1030.
- 678 Grist J., Nicholson S. (2001). A study of the dynamic factors influencing the rainfall
679 variability in the West African Sahel. *J Clim.*, 14(7), pp.1337-1359
- 680 Haarsma RJ, Selten FM, Weber SL, Kliphuis M (2005) Sahel rainfall variability and
681 response to greenhouse warming. . *Geophys Res Lett* 32: L17702.

- 682 Held IM, Delworth TL, Lu J, et al. (2006) Simulation of Sahel drought in the 20th and
683 21st centuries. *Natl. Acad. Sci. U. S. A.*, 103(4), pp.1152–1153.
- 684 Hoerling M, Hurrell J, Eischeid J, Phillips A (2006). Detection and attribution of
685 twentieth-century northern and southern African rainfall change. *J Clim*, 19(16),
686 pp.3989–4008.
- 687 Janjic Z (1994) The Step-Mountain Eta Coordinate Model - Further Developments of the
688 Convection, Viscous Sublayer, and Turbulence Closure Schemes. *Mon Weather Rev*
689 122:927–945. doi: 10.1175/1520-0493(1994)122<0927:TSMECM>2.0.CO;2
- 690 Janjic Z (1996) The surface layer in the NCEP Eta Model. Eleventh Conference on
691 Numerical Weather Prediction, Norfolk, VA, 19-23 August; Amer Meteor Soc,
692 Boston, MA 354–355.
- 693 Janjic ZI (2002) Nonsingular implementation of the Mellor–Yamada level 2.5 scheme in
694 the NCEP Meso model. NCEP office note 437:61.
- 695 Kalnay E, Kanamitsu M, Kistler R, et al. (1996) The NCEP/NCAR 40-year reanalysis
696 project. *Bull Amer Meteor Soc* 77:437–471.
- 697 Kanamitsu M, Ebisuzaki W, Woollen J, et al. (2002) NCEP-DOE AMIP-II Reanalysis
698 (R-2). *Bull Am Meteorol Soc* 83:1631–1644.
- 699 Kawase H, Abe M, Yamada Y, et al.(2010). Physical mechanism of long-term drying
700 trend over tropical North Africa. *Geophys Res Lett*, 37, L09706
- 701 Lin Y, Farley R, Orville H (1983) Bulk Parameterization of the Snow Field in a Cloud
702 Model. *Journal of Climate and Applied Meteorology* 22:1065–1092. doi:
703 10.1175/1520-0450(1983)022<1065:BPOTSF>2.0.CO;2

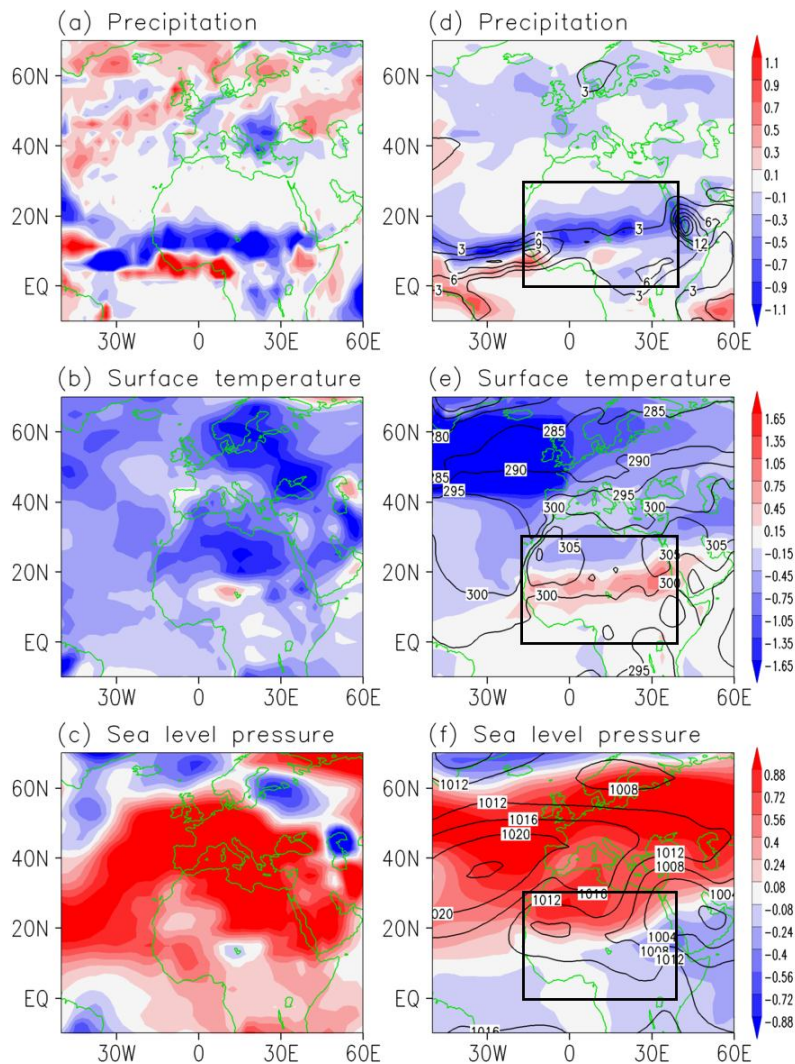
- 704 Liu Y, Chiang JCH (2012) Coordinated Abrupt Weakening of the Eurasian and North
705 African Monsoons in the 1960s and Links to Extratropical North Atlantic Cooling. *J*
706 *Clim* 25:3532–3548. doi: 10.1175/JCLI-D-11-00219.1
- 707 Mlawer EJ, Taubman SJ, Brown PD, et al. (1997) Radiative transfer for inhomogeneous
708 atmospheres: RRTM, a validated correlated-k model for the longwave. *J Geophys*
709 *Res-Atmos* 102:16663–16682. doi: 10.1029/97JD00237
- 710 Monin AS, Obukhov Am (1954) Basic laws of turbulent mixing in the surface layer of
711 the atmosphere. *Contrib Geophys Inst Acad Sci USSR* 151:163–187.
- 712 Mulitza S, Prange M, Stuut JB, et al. (2008) Sahel megadroughts triggered by glacial
713 slowdowns of Atlantic meridional overturning. *Paleoceanography*. doi:
714 10.1029/2008PA001637
- 715 Nicholson S (1979) Revised Rainfall Series for the West-African Subtropics. *Mon*
716 *Weather Rev* 107:620–623. doi: 10.1175/1520-
717 0493(1979)107<0620:RRSFTW>2.0.CO;2
- 718 Nicholson S (2009) On the factors modulating the intensity of the tropical rainbelt over
719 West Africa. *Int J Clim* 29:673–689. doi: 10.1002/joc.1702
- 720 Niedermeyer EM, Prange M, Mulitza S, et al. (2009) Extratropical forcing of Sahel
721 aridity during Heinrich stadials. *Geophys Res Lett*. doi: 10.1029/2009GL039687
- 722 Patricola CM, Cook KH (2008) Atmosphere/vegetation feedbacks: A mechanism for
723 abrupt climate change over northern Africa. *J Geophys Res-Atmospheres*. doi:
724 10.1029/2007JD009608

- 725 Patricola CM, Cook KH (2010) Northern African climate at the end of the twenty-first
726 century: an integrated application of regional and global climate models. *Clim Dyn*
727 35:193–212. doi: 10.1007/s00382-009-0623-7
- 728 Rotstayn LD, Lohmann U (2002) Tropical rainfall trends and the indirect aerosol effect. *J*
729 *Clim*, 15(15), pp.2103–2116.
- 730 Rowell DP, Folland CK, Maskell K, Ward MN (1995) Variability of summer rainfall
731 over tropical north-africa (1906-92) observations and modeling. *Q J R Meteorol Soc*
732 121:669–704. doi: 10.1256/smsqj.52310
- 733 Shanahan T, Overpeck J, Anchukaitis K, et al. (2009) Atlantic Forcing of Persistent
734 Drought in West Africa. *Science* 324:377–380. doi: 10.1126/science.1166352
- 735 Shell K, Kiehl J, Shields C (2008) Using the radiative kernel technique to calculate
736 climate feedbacks in NCAR’s Community Atmospheric Model. *J Clim* 21:2269–
737 2282. doi: 10.1175/2007JCLI2044.1
- 738 Skamarock WC, Klemp JB, Dudhia J, et al. (2008) A description of the Advanced
739 Research WRF Version 3. NCAR/TN-475+ STR
- 740 Smirnova TG, Brown JM, Benjamin SG (1997) Performance of different soil model
741 configurations in simulating ground surface temperature and surface fluxes. *Mon*
742 *Weather Rev* 125:1870–1884. doi: 10.1175/1520-
743 0493(1997)125<1870:PODSMC>2.0.CO;2
- 744 Soden B, Held I, Colman R, et al. (2008) Quantifying climate feedbacks using radiative
745 kernels. *J Clim* 21:3504–3520. doi: 10.1175/2007JCLI2110.1

- 746 Stager J, Ryves D, Chase B, Pausata F (2011) Catastrophic Drought in the Afro-Asian
747 Monsoon Region During Heinrich Event 1. *Science* 331:1299–1302. doi:
748 10.1126/science.1198322
- 749 van Kreveld S, Sarnthein M, Erlenkeuser H, et al. (2000) Potential links between surging
750 ice sheets, circulation changes, and the Dansgaard-Oeschger cycles in the Irminger
751 Sea, 60-18 kyr. *Paleoceanography* 15:425–442. doi: 10.1029/1999PA000464
- 752 Vellinga M, Wood R (2002) Global climatic impacts of a collapse of the Atlantic
753 thermohaline circulation. *Clim Change* 54:251–267. doi: 10.1023/A:1016168827653
- 754 Wang Y, Cheng H, Edwards R, et al. (2001) A high-resolution absolute-dated Late
755 Pleistocene monsoon record from Hulu Cave, China. *Science* 294:2345–2348.
- 756 Xue Y and Jagadish S (1993) The influence of land surface properties on Sahel climate.
757 Part 1: desertification. *J Clim*, 6(12), pp.2232–2245.
- 758 Zhang R, Delworth TL (2005) Simulated tropical response to a substantial weakening of
759 the Atlantic thermohaline circulation. *J Clim* 18:1853–1860.
- 760 Zhang G, Mcfarlane N (1995) Sensitivity of Climate Simulations to the Parameterization
761 of Cumulus Convection in the Canadian Climate Center General-Circulation Model.
762 *Atmos-Ocean* 33:407–446.
- 763 Zhou T, Yu R, Li H, Wang B (2008) Ocean forcing to changes in global monsoon
764 precipitation over the recent half-century. *J Clim* 21:3833–3852.



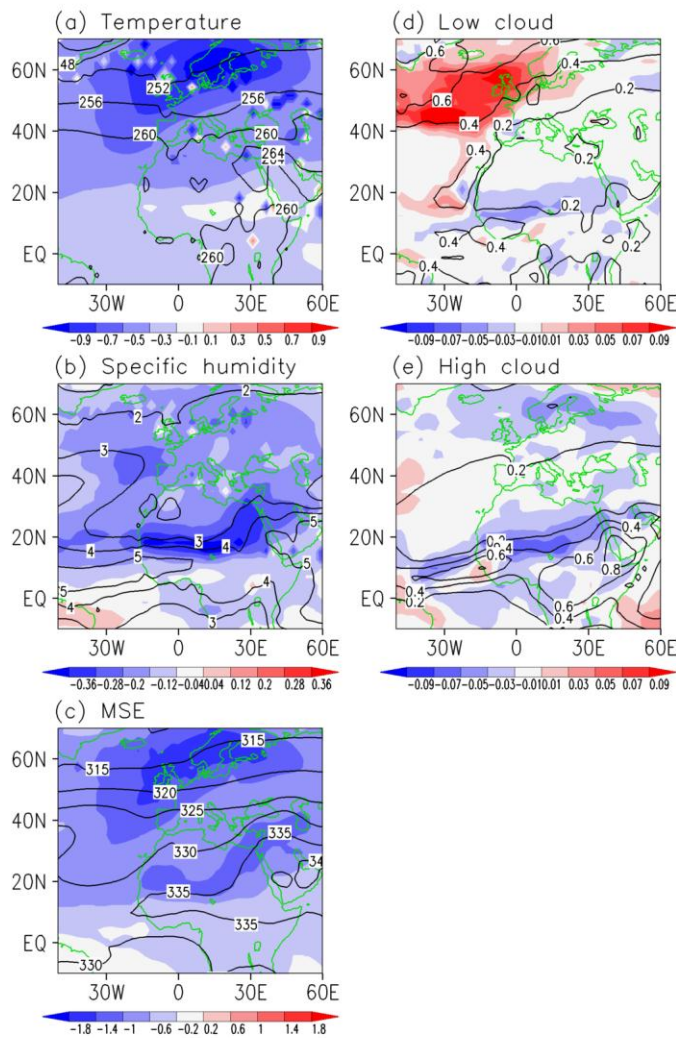
766
 767 **Fig. 1** July through September anomalies from a Community Atmosphere Model 3-slab
 768 ocean simulation, where a 30 W m^{-2} cooling is applied to the slab ocean in the
 769 midlatitude North Atlantic. Both control and cooling simulations were 30 years long, and
 770 the anomalies are derived from the last 20 years. (a) Temperature (shaded; K) and
 771 precipitation (gray contour; interval is 0.5 mm per day, and dashed lines are negative). (b)
 772 Sea-level pressure (shaded; millibars) and lowest-level wind anomalies (reference vector
 773 is 5 m s^{-1} ; only anomalies exceeding 1 m s^{-1} in magnitude shown). The images show the
 774 hemispheric impact of North Atlantic cooling and resulting modification of the tropical
 775 circulation. Adopted from Chiang and Friedman (2012)



776

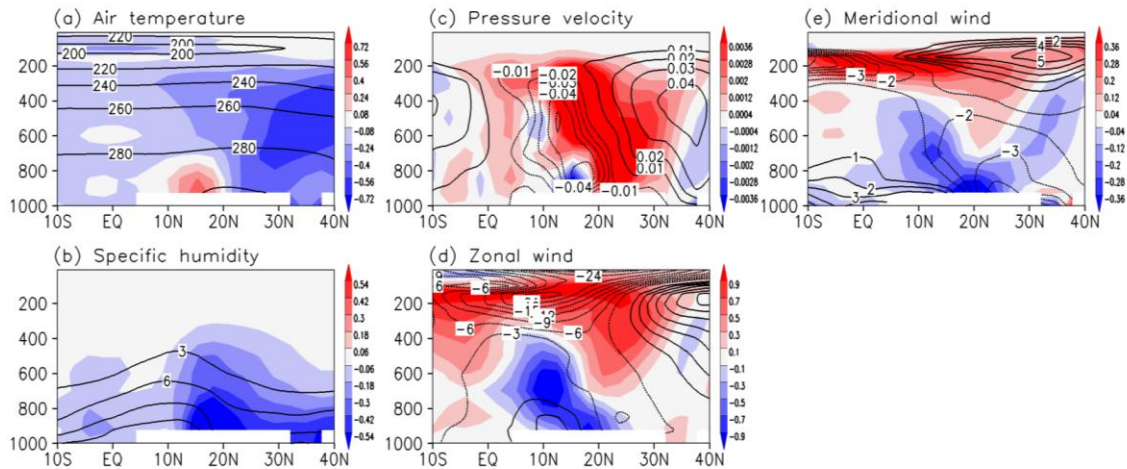
777 **Fig. 2** July through September averaged precipitation (upper panels; mm/day), surface
 778 temperature (middle panels; K) and sea level pressure (lower panels; hPa). Left column:
 779 difference of observed precipitation and reanalysis surface temperature and SLP between
 780 Sahara cold years (1979, 1981, 1984, 1985, 1992, 1993, 1996-1997) and Sahara warm
 781 years (1998-1999, 2001-2003, 2005-2006, 2008). Right column: control run (contour)
 782 and anomalies in the cooling minus control run (shading), in the AGCM simulation using
 783 CAM3.5 coupled with a slab ocean model with 2K cooling prescribed in between 45°

784 60 ° over North Atlantic. Both observation and model simulation show Sahel rainfall
785 reduction, and broad cooling and a SLP increase over Sahara. The color bar for each row
786 is relevant to both panels of the row. The black box denotes the plotted domain of WRF
787 simulation in Fig. 5a-5c. Observations and reanalysis data source: precipitation, GPCP
788 combined precipitation data, developed and computed by the NASA/Goddard Space
789 Flight Center's Laboratory for Atmospheres as a contribution to the GEWEX Global
790 Precipitation Climatology Project (Adler et al. 2003); Surface temperature and SLP:
791 NCEP/NCAR Reanalysis 1 (Kalnay et al. 1996).



792

793 **Fig. 3** July through September averaged (a) mean tropospheric temperature (K), (b) mean
 794 tropospheric specific humidity (g/kg), (c) mean tropospheric moist static energy (kJ), (d)
 795 low cloud coverage (fraction) and (e) high cloud coverage (fraction) in the CAM3.5
 796 simulation for both the control run (contour) and anomalies in the cooling minus control
 797 run (shading)



798

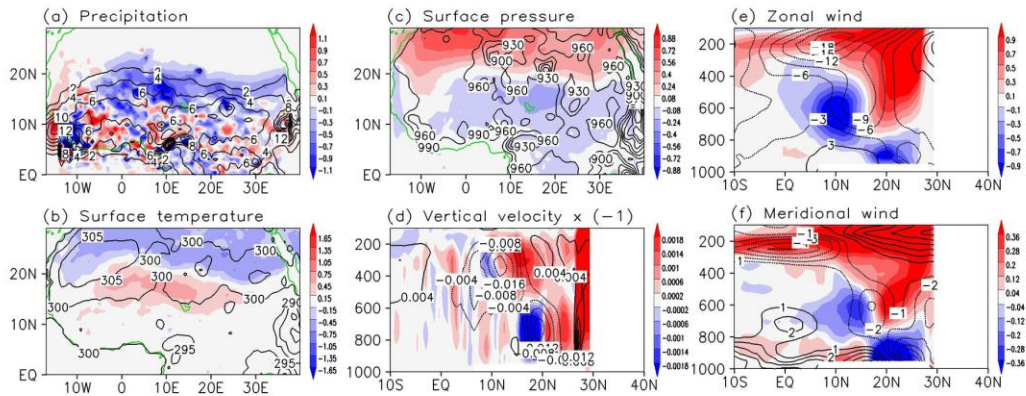
799 **Fig. 4.** Same as Fig. 3 but for pressure-level vertical profile of (a) air temperature (K), (b)

800 specific humidity (g/kg), (c) pressure velocity (Pa/s), (d) zonal wind (m/s) and (e)

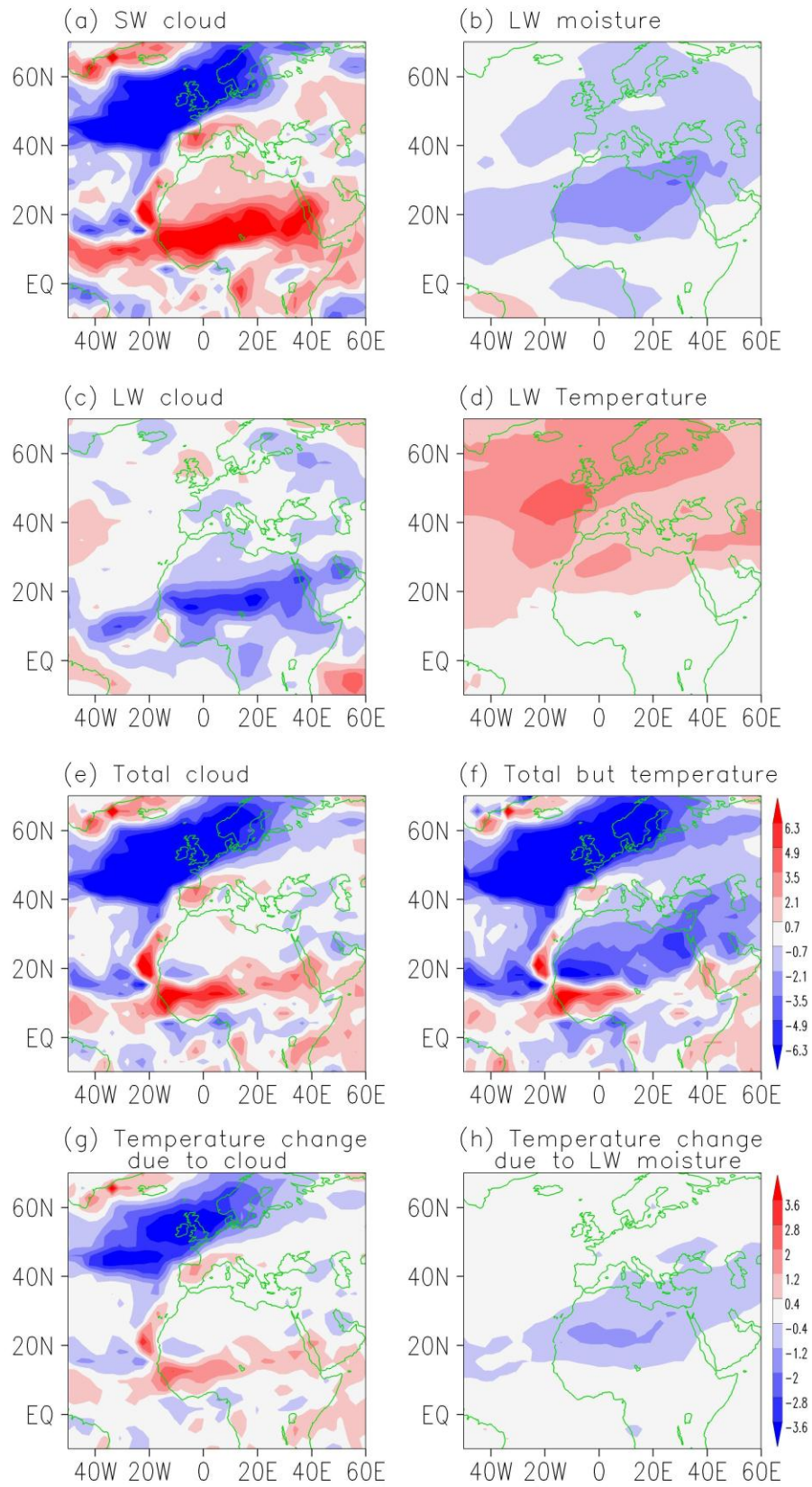
801 meridional wind (m/s). All fields are averaged between 10 °W and 30 °E. Regions of no

802 data (topography) are left blank.

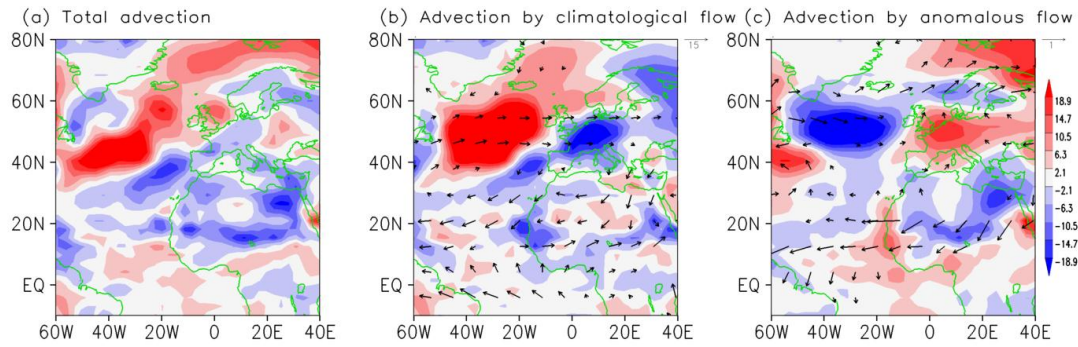
803



804
 805 **Fig. 5.** July-August averaged climate over Africa for the control run (contour) and
 806 anomalies in the experiment (shading) of the WRF simulation with temperature,
 807 geopotential height and relative humidity anomalies from the AGCM cooling runs forced
 808 at the northern boundary of the domain. (a) – (c), surface fields: (a) precipitation
 809 (mm/day), (b) surface temperature (K) and (c) surface pressure (hPa). Only portion of the
 810 domain north of the equator is shown for clarity. (d) – (f), pressure-level vertical profile
 811 of wind component: (d) vertical velocity (multiplied by -1 in accordance with the sign of
 812 pressure vertical velocity; m/s), (e) zonal wind (m/s) and (f) meridional wind (m/s). All
 813 vertical profiles are averaged from 10 °W to 30 °E and the plots are extended to 40 °N to
 814 have the same scale as in Fig. 4. Regions of no data (topography and north of 30 °N in the
 815 plots for vertical profiles) are blank. The WRF cooling simulation generally simulates the
 816 Sahel rainfall reduction, and associated temperature, pressure, and circulation changes as
 817 in the GCM.



819 **Fig. 6** July through September average of TOA Energy flux anomalies due to the
820 feedback of (a) cloud shortwave, (b) moisture longwave, (c) cloud longwave, (d) surface
821 and air temperature longwave, (e) total cloud and (f) total with the exception of
822 temperature, and of partial temperature anomalies due to (g) total cloud feedback and (h)
823 longwave moisture feedback, in the CAM3.5 simulation. The color bar for (a) – (f) is to
824 the right of panel (f), and for (g) – (h) is to the right of panel (h). The units for (a) – (f)
825 are W m^{-2} and for (g) – (h) are K. The figures show that positive cloud (moisture)
826 feedbacks strongly augment the cooling in extratropics (tropics)



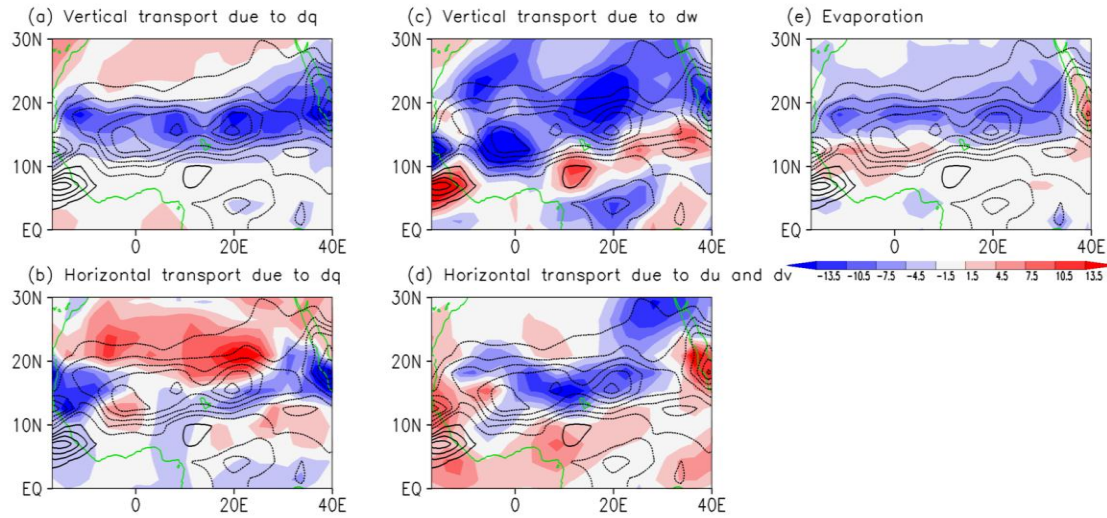
827

828 **Fig. 7** July through September average of vertically integrated horizontal MSE advection829 anomalies in the CAM3.5 simulation (unit: W m^{-2}). (a) total anomaly, (b) the anomaly

830 related to the climatological flow from the control run, (c) the anomaly related to

831 anomalous flow. Arrows are 925mb mean flow (b) and anomalous flow (c) (unit: m/s).

832 The figure shows that the advection of low MSE air cools North Africa.



833

834 **Fig. 8** July through September average of vertically-integrated moisture budget

835 anomalies in the CAM3.5 simulation. Contour: total precipitation anomaly. Shading: (a)

836 vertical moisture transport anomaly due to anomalous moisture, (b) horizontal moisture

837 transport anomaly due to anomalous moisture, (c) vertical moisture transport anomaly

838 due to anomalous vertical wind, (d) horizontal moisture transport anomaly due to

839 anomalous horizontal wind and (e) evaporation anomaly. The unit is $W m^{-2}$. Contour840 interval: $5 W m^{-2}$. The color bar for all panels is at the bottom of panel (e)